

# Tolerance of Silicon Oxide-Coated Pt/C Catalyst Toward CO and H<sub>2</sub>S Contamination in Hydrogen for Proton Exchange Membrane Fuel Cells

Sebastian Prass,\* Leon Nerlich, Rajveer Singh, Andres O. Godoy, Jasna Jankovic, K. Andreas Friedrich, and Nada Zamel\*

Platinum on graphitized low surface area carbon (Pt/C) is coated with a silicon oxide thin film and is employed as anode catalyst to manipulate the tolerance of proton exchange membrane fuel cells toward carbon monoxide and hydrogen sulfide contamination. The SiO<sub>2</sub> coating, prepared by successive hydrolysis of 3-aminopropyl-triethoxysilane and tetraethoxysilane, forms clusters in proximity to Pt in sizes comparable to the catalyst particles, leaving most of the carbon surfaces free. The performance with and without CO is investigated in situ at relative humidities (RH) of 100%, 70%, and 40%. When operated with neat hydrogen, SiO<sub>2</sub>-Pt/C shows marginally better performance owing to an improved protonic conduction due to the water retaining hydrophilic SiO<sub>2</sub>. Upon operation with CO-contaminated fuel, the SiO<sub>2</sub>-Pt/C performs worse than that of Pt/C particularly at high RH. CO stripping measurements reveal an increase in CO oxidation potential for the SiO<sub>2</sub>-Pt/C, suggesting an increased CO coverage and consequently higher anode overpotentials during operation with CO-contaminated fuel. Upon operation with H<sub>2</sub>S in the fuel, the SiO<sub>2</sub> coating extends the lifetime until the cell voltage broke down, which is attributed to the enhanced water retention due to SiO<sub>2</sub> and the solubility of sulfuric species.


reduction reaction (ORR) in the anode and cathode electrodes, respectively, catalysts usually made from platinum group metals (PGM) are employed. As PGM catalysts are one of the main sources for the high costs of PEMFCs, effort is put into lowering the amount or even fully eliminating the use of PGMs by enhancing catalyst and support materials as well as electrode designs to ultimately meet cost, performance, and durability goals.<sup>[1]</sup> Promising materials include platinum (Pt) based alloys with optimized particle distribution or shape selected nanostructures, PGM-free catalysts based on cheaper, less scarce materials, but also catalyst supports with optimized composition and surface morphologies and furthermore ionomers with advanced properties.<sup>[2–4]</sup> The selection of electrode materials in combination with its fabrication process provides many possibilities to influence the efficiency and durability of the PEMFC. In addition to the electrode materials and design, impuri-

ties in fuel and oxidant gas streams constitute another obstacle in meeting the performance and durability goals. A broad spectrum of gaseous or solid, but dissolved species, influence reaction kinetics in the anode and cathode electrodes or impede the mass transport through pores as well as the proton conduction through the electrolyte.<sup>[5]</sup> For the fuel compartment, carbon monoxide

## 1. Introduction

Polymer electrolyte fuel cells (PEMFCs) are a viable alternative to providing zero-emission electricity by conversion of the chemical energy stored in hydrogen via the redox reaction with oxygen. To facilitate the hydrogen oxidation reaction (HOR) and oxygen

S. Prass, L. Nerlich, R. Singh, N. Zamel  
Division Hydrogen Technologies  
Department Fuel Cell  
Fraunhofer Institute for Solar Energy Systems ISE  
79110 Freiburg, Germany  
E-mail: sebastian.prass@ise.fraunhofer.de;  
nada.zamel@ise.fraunhofer.de

 The ORCID identification number(s) for the author(s) of this article can be found under <https://doi.org/10.1002/ente.202300199>.

© 2023 The Authors. Energy Technology published by Wiley-VCH GmbH. This is an open access article under the terms of the Creative Commons Attribution-NonCommercial-NoDerivs License, which permits use and distribution in any medium, provided the original work is properly cited, the use is non-commercial and no modifications or adaptations are made.

DOI: 10.1002/ente.202300199

A. O. Godoy, J. Jankovic  
Materials Science and Engineering Department  
Center for Clean Energy Engineering and Institute for Materials Science  
University of Connecticut  
Storrs, CT 06269, USA

K. A. Friedrich  
Institute of Engineering Thermodynamics  
German Aerospace Center  
70569 Stuttgart, Germany

K. A. Friedrich  
Institute for Building Energetics  
Thermotechnology and Energy Storage  
University of Stuttgart  
70569 Stuttgart, Germany

(CO) inevitably present in hydrogen obtained by reforming plays a significant role as it readily adsorbs on Pt surfaces in the anode electrode, competes with the HOR for active sites, and induces a voltage loss already at low concentrations.<sup>[6]</sup> The tolerance of the anode electrode versus CO contamination can be improved by alloying the Pt catalyst with oxophilic metals such as, e.g., ruthenium (Ru), which either weaken the bond between CO and Pt and/or provide hydroxyl groups (OH) required for CO oxidation.<sup>[7]</sup> Unfortunately, oxophilic metals known to improve the CO tolerance tend to leach out of the catalyst particle leaving a Pt-enriched shell.<sup>[8–13]</sup> Furthermore, these catalysts do not work similarly when it comes to contamination with sulfuric species such as hydrogen sulfide (H<sub>2</sub>S) potentially present in smallest concentrations in hydrogen from decarbonized fossil fuels.<sup>[14]</sup> The dissociative adsorption of H<sub>2</sub>S on electrocatalysts leaves elemental sulfur, which also competes with HOR and results in a complete cell voltage breakdown if no recovery measures are employed.<sup>[15]</sup> Specific recovery protocols but also shut-downs and start-ups can help to recover the PEMFC performance, in which oxygen species and water play central roles for oxidation and dissolution of sulfur species; however, a delay or even elimination of a cell voltage breakdown is preferable.<sup>[16]</sup>

A promising alternative with the potential of addressing both the stability and contamination issues of electrocatalysts are thin functional coatings on catalyst and support particles. Various types of coatings made from organic polymers, inorganic carbon nano-shells, or metal oxide layers fabricated via different chemical or physical deposition processes have shown to either improve stability, selectivity, processability, or the performance of electrocatalysts at specific operating conditions.<sup>[17]</sup> One of these coatings is based on silicon oxide (referred to as SiO<sub>2</sub> hereinafter) applied onto the catalyst via hydrolysis of silicon-containing precursors such as 3-aminopropyl-triethoxysilane (APTES), tetraethoxysilane (TEOS), and methyltriethoxysilane (MTEOS).<sup>[18,19]</sup> When employed on electrocatalysts, such SiO<sub>2</sub> coatings showed to protect the catalysts from dissolution and improved the PEMFC performance particularly at low relative humidity (RH) conditions.<sup>[20–26]</sup> In these regards, Yu et al. used this coating over PtRu catalysts to protect the Ru from dissolution, such that the catalyst maintained the improved CO tolerance during accelerated stress tests.<sup>[20]</sup> Aside from the application as a coating, SiO<sub>2</sub> can also be integrated as an additive to the proton exchange membrane (PEM) or electrode in form of silica particles or aerogel, or as a mesoporous support for the metal catalyst.<sup>[27,28]</sup> If applied as an additive, SiO<sub>2</sub> affects the water retention capacity and PEMFC performance at low RH conditions,<sup>[29,30]</sup> while as a support, it eventually promotes the oxidation of CO on Pt.<sup>[31]</sup> For the latter, the silanol (Si–OH) terminated surfaces of the SiO<sub>2</sub> were found to provide OH groups for CO oxidation, if the catalyst particles were incorporated into the mesoporous structure of the SiO<sub>2</sub>. However, although several features provided by a SiO<sub>2</sub> coating appear promising, the effect of the coating itself on the tolerance of a Pt/C catalyst versus PEMFC fuel contaminants such as CO or H<sub>2</sub>S has not been investigated yet and therefore is objective of this work.

In the present study, commercially available Pt/C was coated with SiO<sub>2</sub> and employed as anode catalyst in PEMFCs operated with CO and H<sub>2</sub>S-contaminated fuel to investigate the effect of the coating on the contaminant tolerance. The underlying

hypothesis of this study is that the SiO<sub>2</sub> either acts as adsorption barrier or that it alters the availability of water and OH groups required for oxidation or dissolution of CO or sulfuric species adsorbed on Pt surfaces, respectively. Transmission electron microscopy (TEM) and scanning electron microscopy (SEM), both coupled with energy-dispersive X-ray spectroscopy (EDX), were employed to examine the structure and composition of the coated catalyst. The effect on performance, ECSA, and CO oxidation potentials were evaluated in a PEMFC operated with CO or H<sub>2</sub>S-contaminated H<sub>2</sub> fuel and Air at various relative humidities (RH).

## 2. Results and Discussion

### 2.1. Structure of SiO<sub>2</sub>-Coated Pt/C

Catalyst particles were analyzed by conventional TEM and STEM-EDX to assess the structure and elemental distribution of SiO<sub>2</sub> on the Pt/C particles. **Figure 1** shows representative particles of both uncoated (Pt/C) and coated (SiO<sub>2</sub>-Pt/C) particles and in the insets magnifications of their carbon support surfaces.

For both, Pt/C and SiO<sub>2</sub>-Pt/C, the dark platinum particles with diameters ranging from 2 to 10 nm are visible on the carbon supports, where they appear to be partly embedded in the multilayer graphene surface. The graphene layers shown in the insets were visible in various thicknesses throughout the carbon surfaces of Pt/C and SiO<sub>2</sub>-Pt/C and cannot be assigned to the SiO<sub>2</sub> coating or an effect of the coating process. For some studies, the SiO<sub>2</sub> coatings could be distinguished from the carbon by their different structures. In case of carbon nanotubes (CNTs) as support, the amorphous SiO<sub>2</sub> could be distinguished from the regular graphene layers by the sheer structure,<sup>[19,21]</sup> whereas for studies employing carbon black (CB) as support, this was rather difficult because the carbon structures were as irregular as the SiO<sub>2</sub> such that the identification of the coating relied on the EDX mappings.<sup>[20,22]</sup> For all these studies, SiO<sub>2</sub> coating thicknesses of few, single digit nanometers were reported either in a homogeneous distribution over catalyst and support material in case of the CNTs or selectively covering the catalyst particles in case of the CB supports. For the present work, the SiO<sub>2</sub> distribution was also qualitatively evaluated from TEM-EDX measurements such as shown in **Figure 2** presenting elemental mappings of C, Pt, Si, and O of the Pt/C and SiO<sub>2</sub>-Pt/C catalysts.

The Pt/C elemental maps show red Pt particles distributed in various sizes on the blue C support, with scattered green Si signals throughout the C and Pt particles. In the EDX spectra of the Pt/C particles, no Si peak (K $\alpha$  lines at 1.74 keV) was visible and therefore the scattered Si signals are considered noise falsely assigned to Si. On the SiO<sub>2</sub>-Pt/C particles, consolidated Si signals in proximity to Pt particles are visible, which in combination of significant Si peaks in the spectra were assigned to SiO<sub>2</sub> clusters that developed on spots favored for condensation of the Si-precursors. From the EDX-maps, SiO<sub>2</sub> clusters in sizes close to Pt particle sizes or layer thicknesses below 1 nm can only be estimated. During the successive hydrolysis of the precursors, the amino groups of APTES should adsorb uniformly over both catalyst and support surfaces dispersed in an alkaline matrix, while TEOS should form the multilayer SiO<sub>2</sub> coating on the

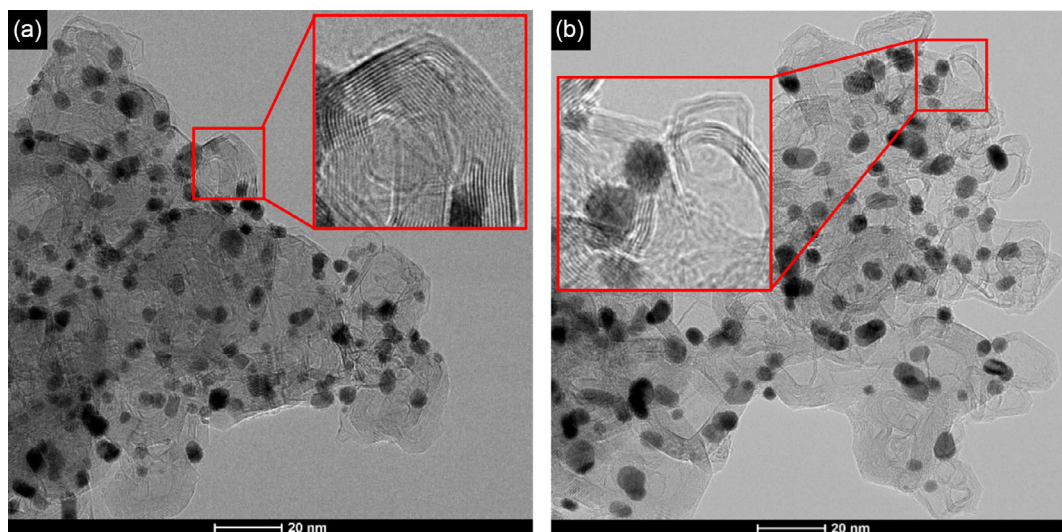


**Figure 1.** TEM image of a) Pt/C and b) SiO<sub>2</sub>-Pt/C particle with insets magnifying the multilayered graphitic carbon support surfaces and black Pt particles appearing partially embedded in the carbon surfaces.

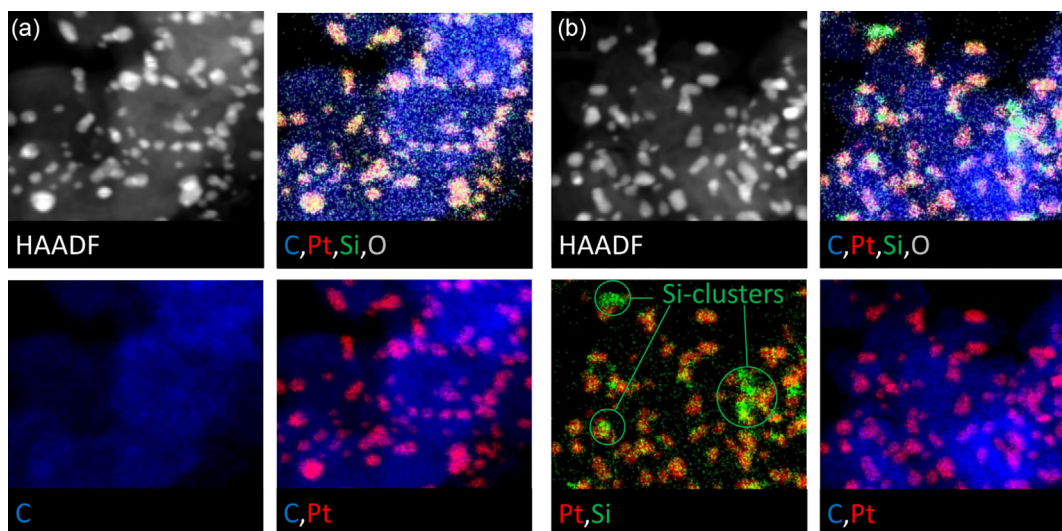


**Figure 2.** TEM-EDX elemental distributions of a) Pt/C and b) SiO<sub>2</sub>-Pt/C particles, the latter showing Si-clusters in proximity to Pt particles.

nucleation sites provided by APTES. The TEM-EDX elemental mappings of multiple samples, however, showed these Si clusters in proximity to catalyst particles with most of the carbon but also Pt surfaces left free. Although this result is different from comparable studies using CNTs with graphitic surfaces as catalyst support, it is expected to be favorable for electron conduction because noncoated carbon surfaces are free of the nonconductive SiO<sub>2</sub> coating, while at least some Pt particles seem to be coated by or in proximity to SiO<sub>2</sub> clusters. From TEM images, the average Pt particle size was determined as  $4.91 \pm 2.2$  and  $5.01 \pm 1.62$  nm for the Pt/C and the SiO<sub>2</sub>-Pt/C catalyst, respectively, with a marginally shifted particle size distribution for the SiO<sub>2</sub>-Pt/C (Figure S1, Supporting Information). The slight shift in particle size distribution for the SiO<sub>2</sub>-Pt/C can be attributed to the

process steps of the SiO<sub>2</sub> deposition; however, the average Pt particle sizes are within the standard deviation and therefore this shift is considered insignificant. In general, the mass activity of electrocatalysts depends on the particle sizes, with a maximum activity at about 2–4 nm for ORR on polycrystalline Pt. This maximum is a result of the balance between strong and too strong adsorption of oxygen species on catalyst surfaces with decreasing particle sizes and a conversely increasing oxophilicity.<sup>[32]</sup> Extrapolated to the anode electrode operated with CO-contaminated fuel, the ability to provide more OH groups required for CO oxidation on smaller catalyst particles could be preferred and consequently, the slight shift in catalyst particle size distribution of the SiO<sub>2</sub>-Pt/C eventually appears disadvantageous.<sup>[33]</sup> On the other hand, SiO<sub>2</sub> surfaces also provide the ability to

**Table 1.** Compositions of Pt/C and SiO<sub>2</sub>-Pt/C catalyst powders from SEM-EDX analysis.

Catalyst	Si [wt.%]	O [wt.%]	Pt [wt.%]	C [wt.%]
Pt/C	0.0	3.3	21.6	74.7
SiO <sub>2</sub> -Pt/C	0.6	3.3	20.3	75.8

forming Si-OH groups from dissociative chemisorption of water or hydronium ions,<sup>[34]</sup> which could benefit the CO or H<sub>2</sub>S tolerance. Here, the morphology difference to the reported studies presumably is a result of the relatively low average Si concentration in the SiO<sub>2</sub>-Pt/C acquired by SEM-EDX (Table 1).

The measured Si loading of ≈0.6 wt% is low as compared to values ranging from 0.3 to 40 wt% reported in other studies on similar types of SiO<sub>2</sub> coatings.<sup>[18,19,21–24,26]</sup> The comparably low concentration is assumed to either stem from adsorption of APTES and TEOS on container surfaces during the coating process or from unreacted reagent removed during the washing procedure at the end of the hydrolysis step. Whether the electrocatalyst stability and performance are enhanced, likely depends on the thickness, pore structure, and hydrophilicity of the SiO<sub>2</sub> coating, being a function of the precursor types, their amount and on the settings during the fabrication process. For example, a hydrogen-rich environment during calcination promotes hydrophobic Si-H rather than hydrophilic Si-OH terminated surfaces, while residual molecules can further exist in the thin film depending on the used precursors.<sup>[19,35]</sup> Coatings made from APTES and MTEOS were found to provide larger and more hydrophobic pore structures owing to methyl groups left in the coating, as compared to coatings made from APTES and TEOS, which can be beneficial for reactant transport and product discharge in the PEMFC cathode. It should be noted that these thin films comprise of non-stoichiometric SiO<sub>2</sub> that interact with the underlying catalyst, features ascribed to the selection of precursors and the calcination step during fabrication.<sup>[20,26]</sup> Generally, for studies with the objective to enhance catalyst stability via SiO<sub>2</sub> coatings, full coverage of the catalyst and support with a thick layer seems advantageous to provide complete protection versus catalyst dissolution and carbon corrosion. If the effect on the performance at varying RH conditions is in focus, thinner layers of SiO<sub>2</sub> could be beneficial, since the surface wettability is already affected by a low SiO<sub>2</sub> content or thin monolayer on the carbon and catalyst surfaces, without altering the diffusion resistances by the coating itself.<sup>[26]</sup> Similarly, a low SiO<sub>2</sub> thickness and consequently loading could suffice to provide the anticipated effect of the coating versus CO and H<sub>2</sub>S contamination, and therefore, these materials were used for the in situ contamination tests.

## 2.2. Electrochemical Characterization of Electrodes

Figure 3 shows CV measurements of the cathode and anode electrodes with and without SiO<sub>2</sub>, with magnified voltammograms of the anode electrodes as well as the ECSA evaluated from H<sub>UPD</sub>. Redox peaks of hydrogen evolution and oxidation reaction (HER and HOR, at potentials <400 mV), Pt oxidation and reduction (>600 mV) as well as double layer charging (400–600 mV) are visible for all CVs. The measured current densities of the anode

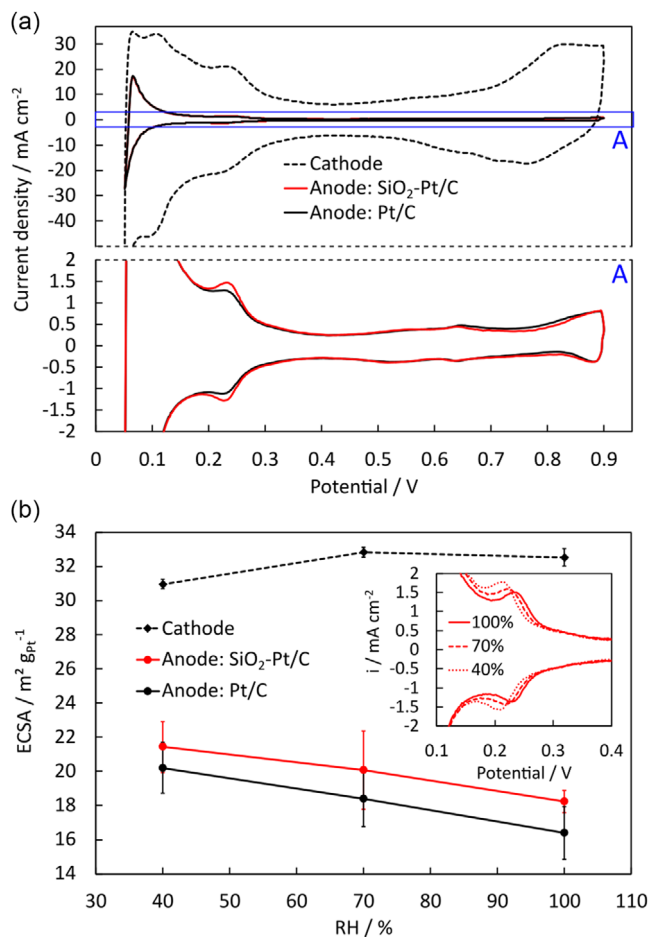


**Figure 3.** a) Cyclic voltammograms of each a cathode and anode electrode with and without SiO<sub>2</sub> at 100% RH and b) average ECSA of all characterized MEAs at 40%, 70%, and 100% RH with the inset showing the changes in the hydrogen adsorption/desorption region associated to the adsorption of SO<sub>3</sub><sup>-</sup> groups.

electrodes are significantly lower as compared to the cathode electrode because the lower loaded anode electrode provides fewer catalyst and support surfaces for the electrochemical processes to occur. This circumstance can create difficulties for evaluation of the anode ECSA because artifact currents such as the signal to noise ratio and relatively augmented HER and HOR of hydrogen evolved in the WE can appear enlarged for low loaded electrodes at potentials less than 0.15 V.<sup>[36]</sup> However, when varying the potentials for integration of the charges transferred, only the magnitudes of the ECSA changed while the trends remained the same. Therefore, the ECSA presented here was evaluated from both hydrogen adsorption and desorption between the typical potentials of 90–400 mV. Consequently, the ECSA is likely overestimated due to increased HER/HOR charges at potentials below 150 mV for both anode electrode types.

From the ECSA, two observations should be noted. First, the ECSA of the SiO<sub>2</sub>-Pt/C and Pt/C increases from ≈18.2 and 16.4 m<sup>2</sup> g<sub>Pt</sub><sup>-1</sup> to ≈21.4 and 20.2 m<sup>2</sup> g<sub>Pt</sub><sup>-1</sup> (corresponding to 17% and 23% increase), respectively, with the decrease in

humidity from 100% to 40%. Usually, the opposite is observed with catalysts on high surface area carbons, where the decrease in ECSA with lower RH is associated to catalyst particles hidden in carbon nanopores or catalyst clusters without contact to the proton conducting ionomer.<sup>[37,38]</sup> At high RH, water on surfaces and in pores inherits the proton conduction and provides the hidden catalyst particles with protons for  $H_{UPD}$ . At low RH, these protonic pathways are absent and such catalyst particles cannot be reached by protons. In this study, a Pt catalyst on graphitized carbon with low surface area was employed, where most of Pt particles are located on the carbon surfaces, ideally in contact with the ionomer and available for  $H_{UPD}$ , if the ionomer is well distributed in the electrode. In such a case, the ECSA would be expected to remain approximately constant across the RH values. However, the ECSA reported here increases, which is a consequence of the shift in the potential and current density of the peaks with lower RH values shown in Figure 3b) inset. We believe that this shift can be attributed to sulfuric acid head groups ( $SO_3^-$ ) of the ionomer, which adsorb and desorb during potential sweeps in the  $H_{UPD}$  region.<sup>[39]</sup> As the adsorption strength of these anionic groups depends on the water content, the charge density at the Pt surfaces varies with RH and creates the observed increase in ECSA when the lower integration limit is kept at 90 mV. The second unexpected observation is that the  $SiO_2$ -Pt/C ECSA is about  $\approx 10\%$  higher than the ECSA of the Pt/C throughout the tested RH conditions, which typically comes with a lower ECSA at equal Pt loading (exact loading values  $75 \pm 4$  versus  $76 \pm 4 \mu g_{Pt} cm^{-2}$  for Pt/C and  $SiO_2$ -Pt/C, respectively). Comparable studies reported a lower ECSA for  $SiO_2$ -coated catalysts and associated this to the coverage of catalyst surfaces by thick  $SiO_2$  coatings limiting the accessibility for reactants.<sup>[20,25]</sup> In the present study, the comparably thin and nonuniformly deposited  $SiO_2$  in combination with its hydrophilic nature, specifically when it stems from hydrolysis of APTES and TEOS,<sup>[19]</sup> could allow for improved water retention in the electrode and, thus, improve protonic connection of Pt particles which are otherwise not in contact to the ionomer. The presence of the low amounts of  $SiO_2$  therefore could lead to an improved accessibility of the catalyst particles. In turn, this would indicate an improper distribution of ionomer indicated by the lower ECSA for the Pt/C electrodes. However, independent of the explanations for the two unexpected observations made with ECSA from  $H_{UPD}$ , the  $SiO_2$ -Pt/C electrodes providing a higher ECSA would be expected to perform better upon operation with CO-contaminated fuel, as the available ECSA is one of the crucial parameters determining the CO and  $H_2S$  tolerances.<sup>[6]</sup>

### 2.3. Performance in Neat $H_2$

Figure 4 shows polarization curves including the HFR of the Pt/C and  $SiO_2$ -Pt/C MEAs operated with neat and CO-contaminated  $H_2$  on the anode and air on the cathode side at RH values of 100%, 70%, and 40%. For better visualization, the insets show the difference in current densities between the MEAs types at three cell voltages of 0.8, 0.5, and 0.2 V resembling activation, ohmic, and mass transport loss dominated regions, with the color signifying which MEA shows better performance.

Upon operation with neat  $H_2$  (Figure 4a)), the MEAs with and without  $SiO_2$  in the anode electrode show an almost similar performance considering the standard deviation represented by the error bars. A slight improvement for the  $SiO_2$ -Pt/C becomes apparent at higher current densities for all RH conditions as emphasized by the insets. This improvement is a consequence of the approximately 1%–3% lower HFR for  $SiO_2$ -Pt/C, resulting in a nearly proportional increase of the differences in current density up to about  $0.06 A cm^{-2}$  at 0.2 V of the polarization curve at 70% RH. Generally,  $SiO_2$  is known to improve water retention due its comparably hydrophilic nature particularly if surfaces are terminated with OH groups, which can be of help especially during low RH operation.<sup>[30]</sup> This beneficial effect though depends on how the  $SiO_2$  is incorporated into the electrodes or the PEM, on its concentration as well as on the operating conditions of the PEMFC. When employed as a coating such as in the present study,  $SiO_2$  can provide improved water retention capabilities, but hinder electron conduction as it was observed in the study by Fujii et al.<sup>[22]</sup> The authors measured an increased HFR and electrode resistivity and attributed it to the electrically insulating character of the  $SiO_2$  coating, which in their case was comparably thick (5 nm), in high concentration (40 wt% silica determined from ICP-AES) and homogeneously distributed also over the carbon support surfaces. At lower concentrations and adjusted ionomer contents in the cathode electrode,  $SiO_2$ -containing MEAs can provide better performances at low RH conditions, but also limited mass transport at high RH values and current densities.<sup>[23,24]</sup> In the present work, the effect on water retention appears to excel effect of the  $SiO_2$  on electronic or reactant diffusion resistances visible in the slightly better performance in neat  $H_2$ .

Upon operation with 1 ppm CO in  $H_2$  (Figure 4b)), the polarization curves show the typical trend with elevated CO concentrations, that is, (1) the regular voltage decay at low current densities arising mainly due to the activation of the catalyst for ORR in the cathode electrode, (2) a relatively sudden drop at voltages below approximately 0.7 V, and (3) the relaxation from the drop at potentials  $< 0.4$  V. Generally, CO strongly adsorbs on Pt and competes with HOR for active sites



At low current densities, the fraction of Pt covered and blocked by CO, being a function of the concentration and the rate of oxidation with OH groups or crossover oxygen, leaves yet sufficient Pt sites vacant to maintain the required HOR.<sup>[40,41]</sup> With higher current densities, the sudden drop arises as a result of the competition between HOR and CO blocking Pt sites, giving rise to a higher anode overpotential and total cell impedance with CO (e.g., Figure S2, Supporting Information, for the case of  $1 A cm^{-2}$ ). With increasing current density, the anode overpotential increases until the anode reaches potentials sufficiently high to accelerate CO oxidation. CO electrooxidation on catalysts such as Pt generally involves water adsorbing and oxidating on active catalyst sites to forming OH groups, which then oxidize adsorbed CO molecules on neighboring catalyst sites:



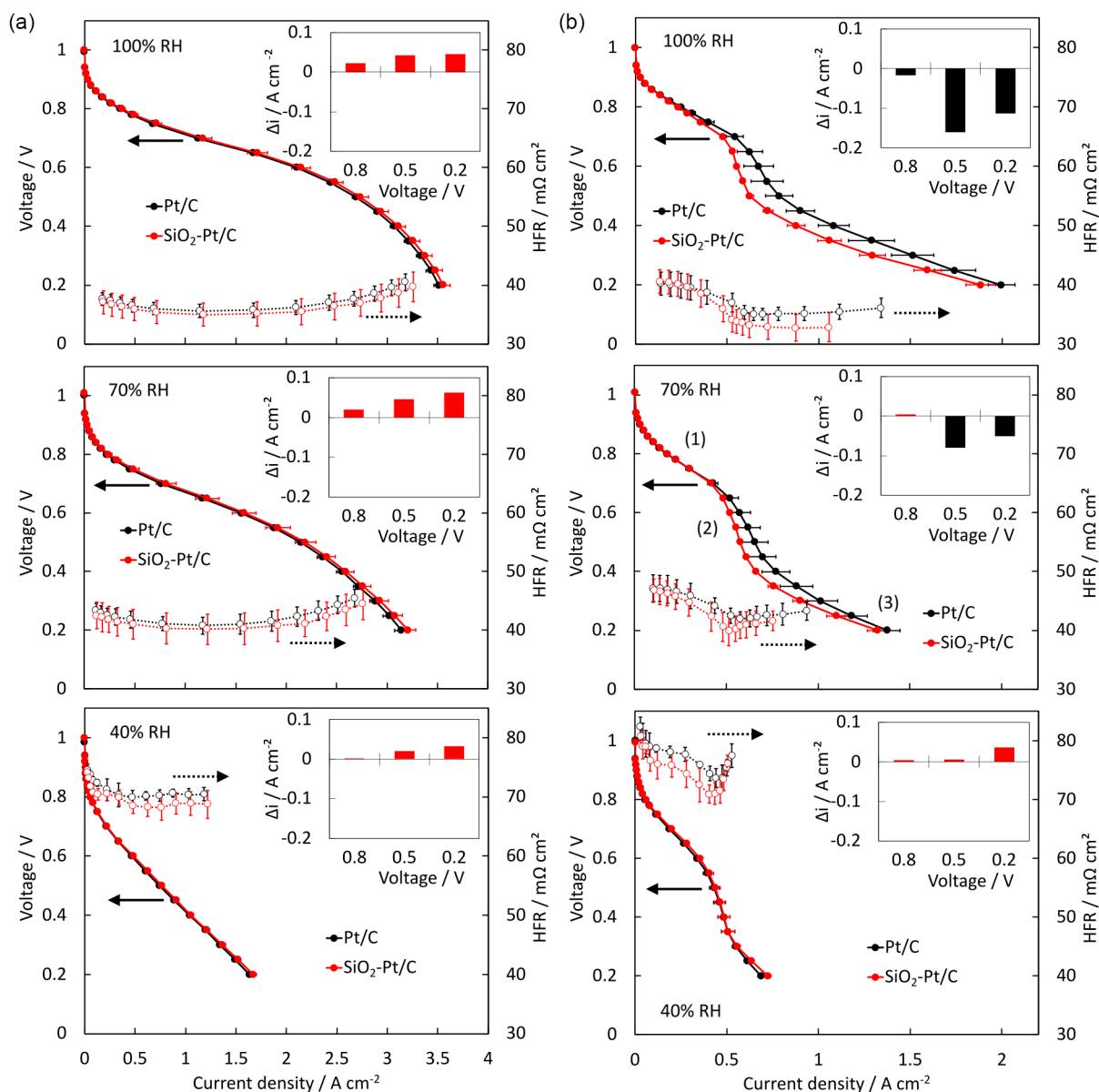
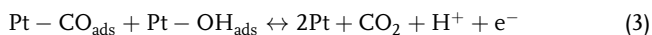


**Figure 4.** Polarization curves and HFR at 100%, 70%, and 40% RH with neat a) H<sub>2</sub> and b) 1 ppm CO supplied to the anode. Insets showing the difference between MEAs with and without SiO<sub>2</sub> coating (red bars—SiO<sub>2</sub>-Pt/C exhibiting better performance).



The kinetics of CO oxidation on Pt and other catalysts depends on several factors such as the surface structures and compositions of both catalyst and its support, the operating temperature, and RH.<sup>[11,42–45]</sup> On Pt, the CO oxidation potential can range from approximately 0.35 to 0.7 V versus RHE for specific facets, with lower potentials indicating that less energy is required to oxidize CO.<sup>[46]</sup> From the polarization curves presented here, SiO<sub>2</sub> being present as a coating in the anode electrode deteriorates the PEMFC performance particularly at elevated RH values. At low current densities <0.5 A cm<sup>-2</sup>, the MEAs perform practically similar; however, the drop in performance due to

CO contamination commences for the SiO<sub>2</sub>-Pt/C MEAs at lower current densities and more abruptly at intermediate potentials (between 0.65 and 0.7 V) at 70% and 100% RH. For all RH values, the HFR of the SiO<sub>2</sub>-Pt/C MEA is lower at higher current densities and equal to the HFR of the Pt/C MEA at low current densities. The differences in current density at a given cell potential decrease with RH, e.g., from approximately 0.15, 0.08, and 0 A cm<sup>-2</sup> at 0.5 V for the polarization curves at 100%, 70%, and 40% RH, respectively. With lower RH, the water retaining and HFR lowering effect of the SiO<sub>2</sub> supersedes the negative effect on CO tolerance, such that the polarization curves at 40% RH are practically similar. These results indicate a negative impact of the SiO<sub>2</sub> coating toward the CO tolerance of the catalyst, which is more prominent than its beneficial effect on the

protonic conductivity of the ionomer at elevated RH values, while for low RH, these trends are counterbalanced. Considering the evaluated 10% higher ECSA for the SiO<sub>2</sub>-Pt/C electrode determined by H<sub>UPD</sub>, the coating must negatively influence the CO oxidation potential to explain this divergence. To evaluate the oxidation potential, CO stripping was conducted at 100%, 70%, and 40% RH with the SiO<sub>2</sub>-Pt/C and Pt/C anode electrodes as WE. **Figure 5** shows the anodic and cathodic potential sweep of the first CV cycle with a focus on the CO oxidation peak between potentials of 0.55 and 0.7 V.

Upon the start of the anodic sweep at 0.1 V, close to zero charge transfer is measured until CO oxidation commences at about 0.55 V. Once CO is oxidized and catalyst surfaces are vacant, HOR of crossover H<sub>2</sub> occurs, until Pt oxides form above 0.7 V and passivate the catalyst for the HOR, resulting in the current density drop between 0.7 and 0.95 V.<sup>[36]</sup> During the reverse cathodic scan, Pt oxide reduction and the resumption of HOR of crossover H<sub>2</sub> occur from 0.8 to 0.6 V, followed by double-layer charging (between 0.3 and 0.5 V) and H<sub>UPD</sub> and HER from 0.3 to 0.1 V. As can be seen in Figure 5b), the potential onset, where the CO oxidation starts, is lower for Pt/C at all RH conditions. The largest difference of approximately 20 mV (0.54 V versus 0.56 V for the SiO<sub>2</sub>-Pt/C) is visible at 100%

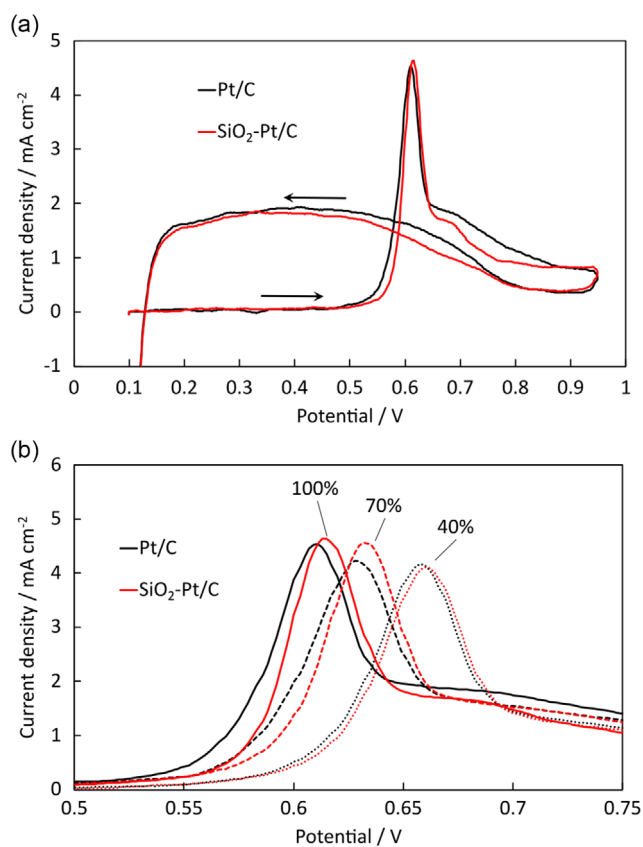


**Figure 5.** CO stripping voltammetry at 20 mV s<sup>-1</sup> sweep rate of Pt/C and SiO<sub>2</sub>-Pt/C electrodes a) at 100% RH and b) magnification on the CO oxidation peaks at three RH values. The CO was preadsorbed at 0.05 V for 10 min to allow for complete CO coverage before commencing the CO stripping.

at 40% RH. Such an increase in CO oxidation potential was also observed by Yu et al., who investigated the stability enhancing effect by a SiO<sub>2</sub> coating on PtRu catalysts.<sup>[20]</sup> This change in the onsets of CO oxidation correlates well to trend in the polarization curves with CO-contaminated fuel measured in this work. Though the CO stripping measurements give no information on the actual CO coverage during PEMFC operation with H<sub>2</sub> and air, they indicate that CO on SiO<sub>2</sub>-coated Pt/C requires more energy to oxidize and therefore will cause higher anode overpotentials. Based on the investigations by Fukuoka et al. on preferential oxidation (PROX) of CO on Pt catalysts supported on various types of (silicon based) materials, the electronic states of CO on Pt surfaces were essentially the same when applied onto different supports, but the activities of the support toward O<sub>2</sub> adsorption and formation of oxygenated species such as silanol were found to vary with the support.<sup>[31]</sup> Projected onto the results presented here, the higher CO oxidation potential and worse PEMFC performance would not stem from a stronger bond of CO on Pt, but rather from interactions between SiO<sub>2</sub> and oxygen species, possibly leading to a hindered formation or mobility of OH on catalyst or support surfaces and consequently to a complete oxidation of CO only at higher potentials. In addition, adsorption of CO on the SiO<sub>2</sub> surface and a spillover onto catalyst sites are possible, which could further add to the observed worse performance of SiO<sub>2</sub>-Pt/C.<sup>[47]</sup> Considering these results in combination with the comparably low Si loading of the SiO<sub>2</sub>-Pt/C, a positive effect of higher SiO<sub>2</sub> loadings on the CO tolerance seems unlikely for the silicon precursors and fabrication procedure used in this work.

#### 2.4. H<sub>2</sub>S Tolerance of SiO<sub>2</sub>-Pt/C

Although the SiO<sub>2</sub> coating negatively affects the performance upon operation with CO-contaminated fuel, an opposite effect was visible with respect to H<sub>2</sub>S contamination. **Figure 6** presents the cell voltage trends of Pt/C and SiO<sub>2</sub>-Pt/C MEAs at constant galvanostatic operation of 1 A cm<sup>-2</sup> and 40% RH with 75 ppb

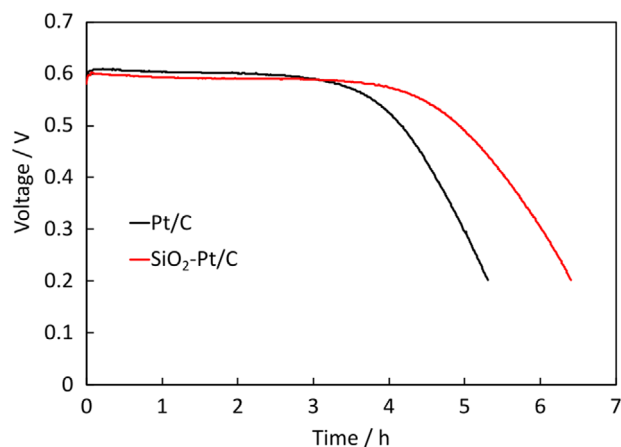
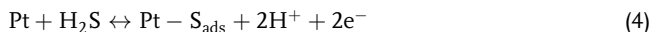


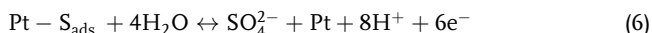
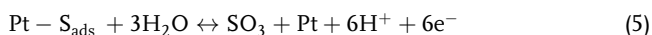
**Figure 6.** Cell voltages of SiO<sub>2</sub>-Pt/C and Pt/C MEAs at 1 A cm<sup>-2</sup> and 40% RH with 75 ppm H<sub>2</sub>S in H<sub>2</sub>, with the typically observed cell voltage breakdown due to sulfur poisoning after several hours of operation.

H<sub>2</sub>S in the fuel showing the typical voltage drop due to sulfur poisoning of the anode electrode.

The multistep dissociative adsorption of H<sub>2</sub>S on Pt (and other electrocatalysts) leaves elemental sulfur, which also competes with the HOR for active catalyst sites:



The oxidation of sulfur on Pt requires significantly higher potentials as compared to the oxidation of CO and typically shows two oxidation peaks occurring between 0.8 and 1.2 V versus RHE during CV measurement of a sulfur-contaminated electrode. These two peaks are assigned to the oxidation of linear and bridge bonded sulfur, i.e., sulfur atoms blocking one or two Pt atoms and requiring more or less energy for oxidation.<sup>[15]</sup> Sulfur adsorbed on Pt catalyst can oxidize with water toward oxidized sulfur species as proposed by Loučka et al.<sup>[48]</sup>



The formation of linear or bridge bonded sulfur depends on temperature and the water content in the electrode, and consequently their oxidation potentials varies with these parameters.<sup>[49,50]</sup> With higher temperatures and RH, the oxidation potential for sulfur on Pt shifts slightly toward lower potentials, e.g., from about 0.96 to 0.84 V versus RHE for the oxidation peak of bridge-bonded sulfur with the increase in temperature from 50 to 90 °C. Although these potentials are typically not reached by the anode electrode unless specific events like fuel starvation or cyclic voltammetry force the potential to such values, the trend with RH points toward the beneficial effect that water has on sulfur contamination in general. This can also be seen during operation of the PEMFC with H<sub>2</sub>S-contaminated fuel, where an increase in the RH extends the durability until the voltage break down occurs.<sup>[51]</sup> During operation, a fraction of the sulfur species eventually reacts toward soluble oxidized sulfur species such as sulfate (SO<sub>4</sub><sup>2-</sup>), allowing for scavenging with liquid water eventually and a partial recovery from the contamination.<sup>[52]</sup> In addition, a spillover of oxidized sulfur species from the Pt catalyst to the SiO<sub>2</sub> surfaces is possible, where further oxidation and formation of sulfate is possible.<sup>[53]</sup> This interaction between oxidized sulfur species and the SiO<sub>2</sub> coating and surface groups could explain the different behavior of the SiO<sub>2</sub> with respect to the tolerance versus CO and H<sub>2</sub>S contamination. Ultimately, the delayed voltage drop of the SiO<sub>2</sub>-Pt/C upon exposure to H<sub>2</sub>S-contaminated fuel indicates a positive influence of the SiO<sub>2</sub> coating, which can be attributed to the enhanced water retention and a facilitated oxidation and dissolution of sulfur species due to the SiO<sub>2</sub> in electrode. However, instead of the rather complex coating process via hydrolysis of silicon containing precursors, the simple addition of silica or aero gel to the anode electrode during paste or ink fabrication could eventually provide a comparable water retaining and potentially H<sub>2</sub>S tolerance enhancing effect, which would have to be confirmed in further investigations.<sup>[29]</sup>

### 3. Conclusion

Pt metal catalyst particles supported on graphitized carbon (Pt/C) have been coated with silicon oxide (SiO<sub>2</sub>) to investigate the effect of the coating on the tolerance versus carbon monoxide (CO) and hydrogen sulfide (H<sub>2</sub>S) when employed as catalyst in the anode electrode of a PEMFC. Small clusters of SiO<sub>2</sub> formed on and in proximity to Pt catalyst particles of comparable sizes, such that most of the carbon and Pt surfaces were uncoated. Despite similar Pt loadings per area, the SiO<sub>2</sub>-Pt/C revealed a larger ECSA evaluated from H<sub>UPD</sub> throughout relative humidities (RH) of 40%, 70%, and 100%, which is associated to the water retaining character of the SiO<sub>2</sub>, affecting the accessibility of Pt particles during CV measurements. Upon operation in neat H<sub>2</sub>, the SiO<sub>2</sub>-Pt/C showed marginally better performance due to a 1%–3% lower cell resistance based on the water retaining character of SiO<sub>2</sub>. However, the performance was worse for the SiO<sub>2</sub>-Pt/C MEAs with 1 ppm CO in the fuel at high RH (70% and 100%), and comparable for low RH (40%) conditions despite the higher anode ECSA. CO stripping measurements revealed elevated onsets of CO oxidation for the SiO<sub>2</sub>-Pt/C particularly at high RH, suggesting either a hindrance of OH formation or of the mobility of CO and OH on the catalyst, which are required for CO oxidation. The SiO<sub>2</sub> coating though extended the durability of the PEMFC upon operation with 75 ppb H<sub>2</sub>S in the fuel by approximately 20%, which can be attributed to the water retaining character of the SiO<sub>2</sub>, and furthermore to interactions between oxidized sulfur species and the coating. Overall, the SiO<sub>2</sub> coating negatively influences the CO tolerance of a Pt/C catalyst, but positively the water retention and coherent protonic resistance, and furthermore the H<sub>2</sub>S tolerance of a PEMFC anode electrode. Hence, side effects such as a diminished or improved tolerance versus specific contaminants or enhanced water retention should be taken into consideration when designing electrodes including SiO<sub>2</sub> coatings of electrocatalysts, which are intended to improve the catalyst stability versus degradation.

### 4. Experimental Section

*Synthesis of the SiO<sub>2</sub>-Pt/C Powder and Fabrication of the Membrane Electrode Assembly (MEA):* Two types of MEAs were fabricated for this study, with the only difference being the anode electrode with or without SiO<sub>2</sub> coating on the carbon-supported catalyst (Pt/C). For the cathode electrodes, Umicore Pt50 0550 catalyst powder with 50 wt% Pt on carbon was used as received. For the anode electrodes, Umicore Pt20 0390 catalyst powder (both types purchased from Umicore) with 20 wt% Pt on graphitized carbon support was used as base material. The anode catalyst powder was coated with SiO<sub>2</sub> by successive hydrolysis of 3-aminopropyltriethoxysilane (APTES) and tetraethoxysilane (TEOS, purchased from Carl Roth Chemicals) without further optimizing the SiO<sub>2</sub> thickness following the procedure by Takenaka et al.<sup>[21]</sup> In brief, catalyst powder (0.7 g) was ultrasonicated in 50% ethanol and deionized (DI) water (1.4 L) for 10 min. The dispersion was heated to 60 °C and the pH adjusted to ≈11 by addition of trimethylamine (TEA, also purchased from Carl Roth Chemicals). APTES (0.077 mmol) was added to the dispersion and stirred for 1 h followed by the addition of TEOS (10.08 mmol) and further stirring for 3 h at 60 °C to allow for the hydrolysis to proceed. After hydrolysis, unreacted reagent was removed by repeated centrifugation and dispersion of the slurry in fresh DI-water. After the washing procedure, the slurry was dried overnight in air before its calcination in nitrogen (N<sub>2</sub>) atmosphere for 3 h at 623 K to obtain SiO<sub>2</sub>-coated Pt/C catalyst denoted



as SiO<sub>2</sub>-Pt/C hereinafter. The reference Pt/C anode catalyst was introduced in a separate vessel in the calcination oven to exert a similar heat treatment and eventual catalyst sintering. The dry SiO<sub>2</sub>-Pt/C powder was ball-milled to breakdown agglomerates and acquire a fine powder before preparation of the catalyst ink for the electrode printing process.

Catalyst pastes for anode and cathode electrodes were prepared in similar manner by mixing the respective catalyst powder (0.6 g) in water and alcohols (ethylene glycol, 1-methoxy-2-propanol) with Aquivion D79—25BS (25 wt% in water, purchased from Sigma-Aldrich Chemie GmbH) using an axisymmetric centrifuge (SpeedMixer, Hauschild GmbH & Co. KG) and magnetic stirring. For all pastes, the same solvents and ionomer content in the electrode (30 wt%) were employed. These pastes were screen printed onto glass fiber-reinforced PTFE decals with target loadings of 0.07 and 0.55 mg<sub>Pt</sub> cm<sup>-2</sup> for anode and cathode electrodes, respectively. Each an anode and cathode decal was hot pressed (at 10 bar and 180 °C for 15 min) onto an automotive PEM (FS-715-RFS chemically and mechanically stabilized membrane with 15 μm thickness received from Fumatech BWT) to fabricate the catalyst-coated membrane (CCM). These CCMs were framed in a gasket (Teonex, purchased from CMC Klebtechnik GmbH) and assembled with two Freudenberg H23C9 gas diffusion layers (GDLs) to form the membrane electrode assembly (MEA).

**Analysis of Catalyst Material:** The elemental compositions of the Pt/C powders with and without SiO<sub>2</sub> were analyzed via scanning electron microscope coupled with energy-dispersive X-ray spectroscopy (SEM-EDX, FEI Quanta 400 with EDAX EDX) at Fraunhofer ISE. Scanning transmission electron microscopy (STEM) with EDX spectroscopy was performed at the University of Connecticut using a Thermo Fisher Scientific Talos F200X STEM, equipped with Bruker Super-X four silicon drift detectors for EDX spectrometry (Super-X SDD EDXS) to acquire structural information and local SiO<sub>2</sub> distribution of the coated Pt/C particles.

**Electrochemical Measurements:** Electrochemical measurements were conducted on an inhouse built testbench (equipped with Zahner Zennium Pro potentiostat and Kikusui PLZ664WA electric load for electrochemical and performance tests) using a baltic HighAmp qCF single cell (12 cm<sup>2</sup> active area and linear flow field). Polarization curves were carried out at 5 and 2 L min<sup>-1</sup> air and H<sub>2</sub> with and without 1 ppm CO from open-circuit voltage (OCV) to 0.2 V in 10 mV (OCV–0.7 V) and 20 mV (0.7–0.2 V) decrements with sufficient hold time per load point until the current remained constant (less than 100 mA min<sup>-1</sup> change, minimum 8 min hold time). For tests with 75 ppb H<sub>2</sub>S-contaminated fuel, the cells were operated at 1 A cm<sup>-2</sup> to provoke a cell voltage breakdown. The ECSA was determined from hydrogen underpotential deposition (H<sub>UPD</sub>) measured via cyclic voltammetry (CV) in H<sub>2</sub> and N<sub>2</sub> atmosphere with the N<sub>2</sub> flow switched off during voltage sweep at a scan rate of 100 mV s<sup>-1</sup>. For the CO stripping measurements, the working electrode (WE) was conditioned with 1% CO in N<sub>2</sub> prior to the potential sweep at a scan rate of 20 mV s<sup>-1</sup>. Electrochemical impedance spectroscopy (EIS) was used for evaluation of the high-frequency resistance (HFR) during polarization curves. All measurements were carried out at 80 °C and RH conditions given in the respective plots in the following sections. For analysis of the anode electrode, the MEA was turned in the cell such that the anode became the WE and the cathode the counter electrode (CE). The polarization curves including HFR and the ECSA from H<sub>UPD</sub> presented here resemble averages of three tested MEAs with the standard deviation as error bars.

## Supporting Information

Supporting Information is available from the Wiley Online Library or from the author.

## Acknowledgements

This work was supported by the German Federal Ministry for Digital and Transport within the project H<sub>2</sub> Fuel, contract No. 03B11014C.

Open Access funding enabled and organized by Projekt DEAL.

## Conflict of Interest

The authors declare no conflict of interest.

## Data Availability Statement

The data that support the findings of this study are available from the corresponding author upon reasonable request.

## Keywords

carbon monoxide, fuel cell anodes, hydrogen sulfide, platinum on carbon catalyst, silicon oxide coating

Received: February 25, 2023

Revised: May 26, 2023

Published online: June 22, 2023

- [1] A. Kongkanand, M. F. Mathias, *J. Phys. Chem.* **2016**, *7*, 1127.
- [2] Y. Sun, S. Polani, F. Luo, S. Ott, P. Strasser, F. Dionigi, *Nat. Commun.* **2021**, *12*, 5984.
- [3] M. Etesami, S. Mehdipour-Ataei, A. Somwangthanaroj, S. Kheawhom, *Int. J. Hydrogen Energy* **2022**, *47*, 41956.
- [4] S. Zaman, M. Wang, H. Liu, F. Sun, Y. Yu, J. Shui, M. Chen, H. Wang, *Trends Chem.* **2022**, *4*, 886.
- [5] X. Cheng, Z. Shi, N. Glass, L. Zhang, J. Zhang, D. Song, Z. S. Liu, H. Wang, J. Shen, *J. Power Sources* **2007**, *165*, 739.
- [6] S. Prass, K. A. Friedrich, N. Zamel, *Molecules* **2019**, *24*, 3514.
- [7] S. M. M. Ehteshami, S. H. Chan, *Electrochim. Acta* **2013**, *93*, 334.
- [8] K. Hengge, T. Gänsler, E. Pizzutilo, C. Heinzl, M. Beetz, K. J. J. Mayrhofer, C. Scheu, *Int. J. Hydrogen Energy* **2017**, *42*, 25359.
- [9] M. Lukaszewski, M. Soszko, A. Czerwiński, *Int. J. Electrochem. Sci.* **2016**, *11*, 4442.
- [10] D. Gubán, A. Tompos, I. Bakos, Vass, Z. Pászti, E. G. Szabó, I. E. Sajó, I. Borbáth, *Int. J. Hydrogen Energy* **2017**, *42*, 13741.
- [11] J. X. Wang, P. He, Y. Zhang, S. Ye, *ECS Trans.* **2014**, *64*, 121.
- [12] R. K. Ahluwalia, D. D. Papadias, N. N. Kariuki, J.-K. Peng, X. Wang, Y. Tsai, D. G. Graczyk, D. J. Myers, *J. Electrochem. Soc.* **2018**, *165*, F3024.
- [13] R. L. Borup, A. Kusoglu, K. C. Neyerlin, R. Mukundan, R. K. Ahluwalia, D. A. Cullen, K. L. More, A. Z. Weber, D. J. Myers, *Curr. Opin. Electrochem.* **2020**, *21*, 192.
- [14] B. M. Besancon, V. Hasanov, R. Benesch, M. Barrio, M. J. Møltnvik, *Int. J. Hydrogen Energy* **2009**, *34*, 2350.
- [15] T. Lopes, V. A. Paganin, E. R. Gonzalez, *J. Power Sources* **2011**, *196*, 6256.
- [16] J. Mitzel, Q. Zhang, P. Gazdzicki, K. A. Friedrich, *J. Power Sources* **2021**, *488*, 229375.
- [17] Q. Liu, M. Ranocchiaro, J. A. Van Bokhoven, *Chem. Soc. Rev.* **2022**, *51*, 188.
- [18] S. Takenaka, T. Arike, H. Matsune, E. Tanabe, M. Kishida, *J. Catal.* **2008**, *257*, 345.
- [19] S. Takenaka, H. Miyamoto, Y. Utsunomiya, H. Matsune, M. Kishida, *J. Phys. Chem. C* **2014**, *118*, 774.
- [20] X. Yu, Z. Xu, Z. Yang, S. Xu, Q. Zhang, Y. Ling, *Nanotechnology* **2018**, *29*, 245401.
- [21] S. Takenaka, N. Susuki, H. Miyamoto, E. Tanabe, H. Matsune, M. Kishida, *J. Catal.* **2011**, *279*, 381.
- [22] K. Fujii, M. Ito, Y. Sato, S. Takenaka, M. Kishida, *J. Power Sources* **2015**, *279*, 100.

- [23] K. Park, M. Goto, M. So, S. Takenaka, Y. Tsuge, G. Inoue, *Catalysts* **2021**, *11*, 1517.
- [24] K. Park, T. Ohnishi, M. Goto, M. So, S. Takenaka, Y. Tsuge, G. Inoue, *Int. J. Hydrogen Energy* **2020**, *45*, 1867.
- [25] N. Aoki, H. Inoue, H. Kawasaki, H. Daimon, T. Doi, M. Inaba, *Electrochem. Soc.* **2018**, *165*, 737.
- [26] H. Su, L. Xu, H. Zhu, Y. Wu, L. Yang, S. Liao, H. Song, Z. Liang, V. Birss, *Int. J. Hydrogen Energy* **2010**, *35*, 7874.
- [27] A. Kumar, V. K. Ramani, *Appl. Catal. B Environ.* **2013**, *138–139*, 43.
- [28] X. Yang, Y. Wang, G. Zhang, L. Du, L. Yang, M. Markiewicz, J. Y. Choi, R. Chenitz, S. Sun, *Appl. Catal. B Environ.* **2020**, *264*, 118523.
- [29] V. S. Velan, G. Velayutham, N. Hebalkar, K. S. Dhathathreyan, *Int. J. Hydrogen Energy* **2011**, *6*, 3.
- [30] A. Kusoglu, A. Z. Weber, *Chem. Rev.* **2017**, *117*, 987.
- [31] A. Fukuoka, J. Kimura, T. Oshio, Y. Sakamoto, M. Ichikawa, *J. Am. Chem. Soc.* **2007**, *129*, 10120.
- [32] E. Antolini, *Appl. Catal. B Environ.* **2016**, *181*, 298.
- [33] M. Arenz, K. J. J. Mayrhofer, V. Stamenkovic, B. B. Blizanac, T. Tomoyuki, P. N. Ross, N. M. Markovic, *J. Am. Chem. Soc.* **2005**, *127*, 6819.
- [34] T. S. Mahadevan, S. H. Garofalini, *J. Phys. Chem. C* **2008**, *112*, 1507.
- [35] L. Chen, X. He, H. Liu, L. Qian, S. H. Kim, *J. Phys. Chem. C* **2018**, *122*, 11385.
- [36] S. Prass, J. St-Pierre, M. Klingele, K. A. Friedrich, N. Zamel, *Electrocatalysis* **2020**, *12*, 45.
- [37] H. Iden, A. Ohma, *J. Electroanal. Chem.* **2013**, *693*, 34.
- [38] K. K. D. Malevicha, E. Halliopa, B. A. Peppleya, J. G. Pharoaha, *ECS Trans.* **2008**, *16*, 1763.
- [39] T. R. Garrick, T. E. Moylan, V. Yarlagadda, A. Kongkanand, *J. Electrochem. Soc.* **2017**, *164*, F60.
- [40] J. St-Pierre, *J. Electrochem. Soc.* **2009**, *156*, B291.
- [41] Y. Matsuda, T. Shimizu, S. Mitsushima, *J. Power Sources* **2016**, *318*, 1.
- [42] R. W. Lindström, K. Kortsdottir, M. Wesselmark, A. Oyarce, C. Lagergren, G. Lindbergh, *J. Electrochem. Soc.* **2010**, *157*, B1795.
- [43] S. Rudi, C. Cui, L. Gan, P. Strasser, *Electrocatalysis* **2014**, *5*, 408.
- [44] T. Unmüssig, J. Melke, A. Fischer, *Phys. Chem. Chem. Phys.* **2019**, *21*, 13555.
- [45] M. C. O. Monteiro, L. Jacobse, M. T. M. Koper, *J. Phys. Chem. Lett.* **2020**, *11*, 9708.
- [46] P. Urchaga, S. Baranton, C. Coutanceau, G. Jerkiewicz, *Langmuir* **2012**, *28*, 3658.
- [47] M. Eriksson, L. G. Petersson, *Surf. Sci.* **1994**, *311*, 139.
- [48] T. Loučka, *J. Electroanal. Chem. Interfacial Electrochem.* **1971**, *31*, 319.
- [49] R. Mohtadi, W. K. Lee, J. W. Van Zee, *Appl. Catal. B Environ.* **2005**, *56*, 37.
- [50] Y. Nagahara, S. Sugawara, K. Shinohara, *J. Power Sources* **2008**, *182*, 422.
- [51] F. Uribe, I. Urdampilleta, T. Rockward, E. L. Brosha, F. H. Garzon, *ECS Meet. Abstr. MA2007-02*, Washington, DC **2007**, p. 446, <https://doi.org/10.1149/ma2007-02/9/446>.
- [52] J. St-Pierre, B. Wetton, Y. Zhai, J. Ge, *J. Electrochem. Soc.* **2014**, *161*, E3357.
- [53] D. Bounechada, Z. Darmastuti, M. Andersson, L. Ojamäe, A. Lloyd Spetz, M. Skoglundh, P.-A. Carlsson, *J. Phys. Chem. C* **2014**, *118*, 29713.